Published in final edited form as:
J Comp Physiol B. 2010 April ; 180(4): 599–617. doi:10.1007/s00360-009-0422-9.

Seasonal Protein Changes Support Rapid Energy Production in Hibernator Brainstem

L. Elaine Epperson[1], **James C. Rose**[1], **Rae L. Russell**[1], **Mrinalini P. Nikrad**[1], **Hannah V. Carey**[3], and **Sandra L. Martin**[*,1,2]

[1] Department of Cell and Developmental Biology, University of Colorado School of Medicine, P.O. Box 6511, mail stop 8108, Aurora, Colorado 80045

[2] Program in Molecular Biology, University of Colorado School of Medicine, Aurora, Colorado 80045

[3] Department of Comparative Biosciences, University of Wisconsin-Madison, 2015 Linden Dr., Madison WI 53706

Abstract

During the torpor phase of mammalian hibernation when core body temperature is near 4°C, the autonomic system continues to maintain respiration, blood pressure and heartbeat despite drastic reductions in brain activity. Additionally, the hibernator's neuronal tissues enter into a protected state in which the potential for ischemia-reperfusion injury is markedly minimized. Evolutionary adaptations for continued function and neuroprotection throughout cycles of torpor and euthermia in winter are predicted to manifest themselves partly in changes in the brainstem proteome. Here we compare the soluble brainstem protein complement from six summer active ground squirrels and six in the early torpor phase of hibernation. Thirteen percent of the ~1500 quantifiable 2D gel spots alter significantly from summer to early torpor; the proteins identified in these differing spots are known to play roles in energy homeostasis via the tricarboxylic acid cycle (eight proteins), cytoarchitecture and cell motility (14 proteins), anabolic protein processes (13 proteins), redox control (11 proteins) and numerous other categories including protein catabolism, oxidative phosphorylation, signal transduction, glycolysis, intracellular protein trafficking and antiapoptotic function. These protein changes represent, at least in part, the molecular bases for restructuring of cells in the brainstem, a shift away from glucose as the primary fuel source for brain in the winter, and the generation of a streamlined mechanism capable of efficient and rapid energy production and utilization during the torpor and arousal cycles of hibernation.

Keywords

Thirteen-lined ground squirrel; *Spermophilus tridecemlineatus*; *Ictidomys tridecemlineatus*; DIGE proteomics; hibernation

Introduction

The yearly thermoregulatory cycle of a ground squirrel includes two phases. The summer active phase is similar to that of any non-hibernating homeothermic mammal in that the core body temperature (T_b) is maintained at ~35–37°C. In contrast, the winter phase is characterized by dramatic heterothermy in which T_b drops to ~ −3°C to 5°C (torpor) with the exception of spontaneous arousals to euthermy for ~12–15 hr every 3–16 days (Fig. 1).

[*]corresponding author: Sandy Martin, Sandy.Martin@UCDenver.edu, phone: (303) 724-3467, fax: (303) 724-3420.

In addition to low body temperature, the torpid animal demonstrates a tremendously reduced rate of metabolism, respiration and cardiac rhythm (reviewed in Andrews 2007; Carey et al. 2003; reviewed in Lyman et al. 1982).

Life-sustaining brainstem activity, including regulation of heartbeat, respiration and blood pressure, must meet demands throughout the varied and dynamic phases of hibernation, and indeed distinct patterns of brainstem activity are found in torpor and arousal cycles (Bitting et al. 1994; Bratincsák et al. 2007; Kilduff et al. 1990; Kilduff et al. 1982; Milsom et al. 1999). Additionally, brain tissue assumes a state of protection in hibernation. Hippocampal slices tolerate hypoxia and aglycemia (Frerichs and Hallenbeck 1998), the inflammatory response to traumatic brain injury is minimal (Zhou et al. 2001), neuronal damage does not accrue after cerebral ischemia by cardiac arrest (Dave et al. 2006), and as metabolic rate and T_b increase during arousal from torpor, brain tissues undergo a period of mild hypoxia but remain resistant to stress and damage (Ma and Wu 2008; Ma et al. 2005; Tøien et al. 2001). Shifts in brain activity, cytoarchitecture (Arendt et al. 2003; Ruediger et al. 2007; von der Ohe et al. 2007), energy demand and protection from damage are likely to result from seasonal alterations in gene expression.

Broad-spectrum unbiased screens for changes in gene expression in hibernating sciurids across the annual cycle have been performed at the mRNA level in a variety of tissues including liver, heart, brain (reviewed in Andrews 2007; reviewed in Carey et al. 2003), and five tissues of the arctic ground squirrel (Yan et al. 2008). At the protein level, differences have been detected in hibernators using liver, heart, muscle and intestinal tissues (Eddy et al. 2005; Epperson et al. 2004; Lee et al. 2008; Martin et al. 2008; Russeth et al. 2006). Current data support a two-switch model (Serkova et al. 2007) in which a reprogramming of gene expression is the primary facilitator of the first switch from summer to winter, and the less time- and energy-consuming regulation of small biomolecules controlling protein activity drives the second switch of arousal and torpor.

To better understand the molecular events that underlie the hibernator's ability to maintain neuronal function and resist damage from the extreme changes associated with winter heterothermy, we used a quantitative 2D gel approach to compare the proteins present in summer active (SA) ground squirrel brainstem to those in early torpor (ET). Many of the changes found are consistent with the known dramatic restructuring of cellular architecture. In addition, the ET animals demonstrated steady-state upregulation of proteins in the pyruvate dehydrogenase complex, tricarboxylic acid cycle, and oxidative phosphorylation pathways and downregulation of proteins involved in glucose metabolism. Based on these protein alterations, a model is proposed to explain the remarkable ability of hibernators to meet brain ATP requirements during arousal.

Methods

Animals and acquisition of tissue

Thirteen-lined ground squirrels (*Ictidomys tridecemlineatus*, recently revised from genus *Spermophilus* (Helgen et al. 2009)) were trapped in the summer in the vicinity of Madison, Wisconsin, and were housed, abdominally implanted with telemeters, and euthanized as described previously, (Fleck and Carey 2005). SA animals were anesthetized with isoflurane and decapitated in late June-August when $T_b \approx 37°C$, ET animals after at least 4 torpor-arousal cycles and within 24h of having cooled to a T_b of 5–7°C. Brainstems (pons and medulla only) were removed and snap frozen in liquid nitrogen. The University of Wisconsin Institutional Animal Care and Use Committee approved all animal procedures. The tissues were shipped on dry ice to the University of Colorado and stored at −80°C until use.

Sample preparation

Frozen brainstem was pulverized in liquid nitrogen. Approx. 100mg of frozen powdered tissue was taken from the total, placed in homogenization buffer and processed as previously described for liver in a Polytron (Brinkmann) (Epperson et al. 2004). The homogenate was transferred to a microfuge tube and nuclei were pelleted at 500Xg, 4°C for ten min. The post-nuclear supernatant was gently transferred to another tube and divided into 15μl aliquots. These were snap frozen in liquid nitrogen and stored at -80°C. Each aliquot was used only once to avoid freeze-thaw cycles. One aliquot from each animal was used for protein quantitation by BCA protein assay (Pierce). To prepare the reference standard, 230 μg of each sample (12 total: six SA, six ET) were combined into a single tube and mixed thoroughly. This pooled sample was divided into five aliquots, snap frozen and placed at −80°C until use.

90μg of each sample were denatured overnight at room temperature in denaturing buffer: 8M urea, 2M thiourea, 4% CHAPS, 25mM Tris pH 8.8, and subsequently labeled with Cy2, Cy3 or Cy5 (GE Healthcare). Cy2 was always used to label the reference standard and Cy3 and Cy5 were alternated between SA and ET samples to control for dye bias (“dye swap”). Labeling was done according to the manufacturer’s protocol except that 80nmol rather than 400nmol was used to label 50μg of protein. For each gel, the Cy3 and Cy5-labeled samples were combined with the reference standard (Cy2) and this combined sample was methanol/chloroform precipitated as described (Epperson et al. 2004). The pellet was resuspended in 150μl iso and 150μl 3; iso: 9M urea, 4% CHAPS, 65mM DTT, 35mM Tris base, 0.0025% bromophenol blue. 3: 7M urea, 4% CHAPS, 100mM DTT, 0.0025% bromophenol blue, 2M thiourea, 0.8% 3.5–10 ampholytes (“Resolyte”, Gallard-Schlesinger, Plainview, NY), pipetted 10X with a gel loading tip and shaken at 900rpm, 25°C in a Thermomixer (Eppendorf) for at least two hr to solubilize.

Two-dimensional gel electrophoresis

The solubilized proteins were used to swell Immobiline DryStrips pH 3–10 NL, 18cm (GE Healthcare) for 21–24h at RT, after which isoelectric focusing (IEF) and 2D separation were conducted as previously detailed (Bernard et al. 2004) with 20mg/ml fresh DTT in water added to the basic end filter paper. The IEF program was as follows with 2mA and 5W for all steps: 1) ramp to 500V, 30 min, 2) ramp to 3500V, 4hr, 3) hold at 3500V, 14–17hr total. After focusing, the strips were incubated 15 min each in reducing (50mM Tris pH 6.8, 2% SDS, 15% glycerol, 6M urea, 1% DTT) and alkylating (50mM Tris pH 6.8, 2% SDS, 15% glycerol, 6M urea, 1.25% iodoacetamide, 0.05% bromophenol blue) buffers to covalently modify sulfhydryl groups and prevent subsequent disulfide bridge formation. For the second dimension, proteins were separated by SDS-PAGE on a 9–16% acrylamide gradient, and gels were scanned in the glass plates within four hours of completion of electrophoresis.

Three channels were used on a Typhoon 9400 (GE Healthcare) to collect the Cy2, Cy3, and Cy5 images. For each gel image, a prescan was performed and the photomultiplier voltage adjusted until the spot of maximum volume on each image was reduced to approximately one-third of saturation. Images used for analysis were collected at a pixel size of 100μm. Two of these six gels were “pick” gels that were affixed to glass plates previously marked with reference markers (GE Healthcare, product #18-1143-34) and treated with bind-silane (PlusOne, GE Healthcare) for the purpose of accurate robotic picking and digestion of the protein spots. These two gels were fixed and stained with Sypro Ruby (BioRad) according to Epperson, et al. after scanning for Cy2, 3 and 5 (Epperson et al. 2004).

All 20 images (six gels with three Cy images each: Cy2, Cy3 and Cy5, and two of these same gels poststained with Sypro Ruby to make pick gel images) were imported into

DeCyder 2D 6.5 software (GE) for spot matching. T-tests were run using the Cy images in which the Cy3 and Cy5 spot values (pixel volumes) were normalized to their corresponding Cy2 spot value. The BVA module also includes a statistical post hoc algorithm "False Discovery Rate" (FDR) (Benjamini and Hochberg 1995) which is a stringent modifier of p-values and greatly reduces false positives in a large set of comparisons with a relatively small sample size, the resulting probability is called a "q value". Only spots whose t-tests retained $q \leq 0.05$ that were found to be reproducible and robust by individual inspection on all Cy2 images were excised for identification.

Spot picking and mass spectral analysis

Picks and digests were done in the UCDHSC Proteomics Shared Facility (hsc-proteomics.uchsc.edu/mscore) using an Ettan spot picker and an Ettan spot digester (GE Healthcare). Tryptic fragments were separated in a 3–45% hydrophobicity gradient of buffer B (90% ACN, 0.1% formic acid) over 45 min, followed by a 5 min wash in 90% ACN for analysis of full and tandem mass spectra by LC-MS/MS in an ESI ion trap (LC/MSD XCT Plus, Agilent Technologies) in positive ion mode in the Ultra Scan setting. A full MS scan was followed by tandem mass spectral (MS/MS) scans of the two highest peaks with a dynamic exclusion of 1 min. Raw mass spectra were analyzed using Spectrum Mill MS Proteomics Workbench Rev A.03.02.060a ETD-65. The range of mass limits for the precursor ions was 600–4000 Da, parent and fragment masses were both set to monoisotopic, precursor peptide mass tolerance was 2.5 Da, fragment ion tolerance was 0.7, the enzyme specified was trypsin, maximum number of internal missed cleavage sites was two, and cysteines were given a fixed modification of +57 for carbamidomethylation. The database used was an in-house compilation of all mammal sequences in the NCBI nr database in August 2008 and contained 704,905 entries. Spectral data from the same spot on the two pick gels were combined to increase confidence in the identification.

Protein identifications and functional assignments

Protein IDs were acquired for each spot. A program called ExtracTags was written in-house to collate necessary information from Spectrum Mill results about the peptides on which protein IDs were based. For each peptide, the NCBI GI#, species of the organism to which that peptide was matched, predicted peptide sequence, Spectrum Mill score, SPI (scored peak intensity), parent mass and charge, and delta mass were all recorded. For each protein ID obtained, a combined score from all peptides and the total amino acid coverage by those peptides were also calculated. In all tables, protein IDs relying on a single peptide match were eliminated along with any IDs that were > ±15% of their predicted molecular weight based on the second dimension size. Additionally, for spots with multiple credible identifications where one protein's peptides demonstrated an average spectral intensity that exceeded those of another protein in the same spot by four fold or more, the protein with lower average spectral intensity was discarded (Martin et al. 2008). If the difference in both score and coverage was four-fold or greater, the lower quality identification was discarded. Trypsin and keratin were eliminated from the lists. Identifications that passed these criteria were considered valid, and spots with single valid protein IDs after these eliminations were considered unique IDs. In cases where a protein was "hypothetical" or "unnamed protein product", the name of the human homolog as found using the NCBI BLink blast tool was used. Potential biological function was determined using NCBI's Entrez Gene and links therein.

Western blot analysis

20μg of total brainstem protein were separated by SDS-PAGE. One of the SA samples had been depleted and was therefore omitted from the western blot analysis. The gel was cut at the 43kDa marker. The lower portion was stained using Sypro Ruby (Bio-Rad) and scanned

on a Typhoon 9400 (GE) to assess gel loading consistency among lanes. Proteins in the upper gel portion were transferred to Immobilon-FL transfer membrane (Millipore), which was blocked with 3% milk, 1% BSA in TBST and incubated with OGDH goat polyclonal antibody (1:100, SC-49589, Santa Cruz Biotech) at 4°C overnight followed by anti-goat Cy5-conjugated secondary antibody (1:400, Jackson ImmunoResearch). The image was captured using a Typhoon 9400 and analyzed with ImageQuant software.

Results

Protective and functional alterations in the brain are likely to manifest themselves in large part at the protein level in a manner that is dependent on hibernation season (Epperson and Martin 2002; Martin and Epperson 2008; von der Ohe et al. 2007; Zhao et al. 2006). Evidence from previous two-dimensional gel electrophoresis (2DE) studies suggests a loss of protein quality during torpor that is corrected during interbout arousal (Epperson et al. 2004; Martin et al. 2004). Therefore, animals in ET were used in the present study to represent the brainstem proteome of the winter season. Soluble brainstem proteins from six SA and six ET animals were resolved first by isoelectric point and then by size using CyDye labels and 2DE to assess changes in the brainstem proteome associated with the summer to winter alterations in hibernation biochemistry (Fig. 2). Biological replicates were labeled and subjected to 2DE separately rather than pooled to increase statistical power (Karp et al. 2005). The DIGE approach includes a pooled reference labeled with Cy2 which acts as a common denominator, improving quantitation and gel matching (reviewed in Marouga et al. 2005). The most populated gel, the “master” was determined to have 2314 Cy2 spots; these spots were matched to the other Cy2 images allowing for quantitative analysis of their respective Cy3 and Cy5 spots by analysis of their ratios to Cy2, i.e. Cy5/Cy2 compared to Cy3/Cy2 for a single spot. T-tests were run on 2196 spots according to the algorithm present in the DeCyder software. A post hoc multiple test correction algorithm (False Discovery Rate, FDR) was applied to reduce the occurrence of false positives, and only spots that passed this stringent filter were considered further. 633 of the 2196 t-tests demonstrated a p-value of less than 0.05; 286 of these remained significant after FDR ($q< 0.05$).

Of the 286 significantly changing spots, 206 were found to match well on the pick gels and to be reproducible on all gels. These 206 were picked, digested, and their tryptic peptides analyzed by LC-MS/MS mass spectrometry. Protein identifications were obtained for all but seven of the 206 spots analyzed. Information about each uniquely identified protein gene product was found using NCBI’s “Gene” link, and possible functional roles are listed in Tables 1 and 2. 102 (51%) of the 199 identified spots were up in ET relative to SA, 58 of which gave a unique protein ID. 97 (49%) of the 199 identified spots were down in ET, 61 of which gave a unique protein ID. Eighty spots contained multiple valid IDs. Because protein identification by this method depends on the availability of sequence information, the lack of a sequence database for this or a closely related organism lowers the recovery of exact matches. However, high quality spectral information and use of the largest mammalian database available enable positive identification of almost all protein spots with current methods (Epperson et al. 2004; Russeth et al. 2006). One hundred nineteen spots contained a single protein and these unique IDs are reported in Tables 1 and 2. Further information regarding these spots and their corresponding peptides is listed in the Supplementary Table. The fold changes for those spots that were elevated in ET were on average 17% higher than those spots found to be higher in SA ($p<3X10^{-9}$, Student’s t-test; average fold change for ET, 1.55X; for SA, 1.33X). Eighty spots revealed the presence of multiple robust protein identifications, consistent with the high complexity of the starting sample. Proteins identified as changing in steady-state level encompassed many functions including roles in the citric acid cycle, cellular architecture, intracellular transport, protein metabolism and ATP synthesis.

In all cases except two, when more than one spot contained the same protein, those spots were either elevated or reduced coordinately from SA to ET. Only guanine nucleotide binding protein (GNAO1) and aconitase 2 (ACO2), showed a disparate expression: for GNAO1, spots 1167, 1174, and 1176 were elevated in ET (Table 1), and spot 1127 was reduced in ET (Table 2); in the case of ACO2, spot 396 was elevated in ET (Table 1), and spots 318 and 332 were reduced in ET (Table 2). These isoforms likely represent alternative post-translational modifications or a variation earlier in the gene expression process such as alternative splicing.

OGDH, uniquely identified in seven 2D gel spots (Table 1), was selected for verification of the DIGE results by western blotting. Two bands of ~114 kDa were detected with a combined increase in ET of 1.4 fold (Fig. 3). While the results of western blotting are consistent with the DIGE results, the 2D gel method is able to discriminate and independently quantify the significant fold changes for seven different isoforms of the same protein in contrast to the western blot which merges all of these variants of distinct charge (Fig. 2) into two poorly-resolved bands.

The proteins that altered significantly between ET and SA demonstrated consistently small fold changes, with the majority less than two-fold. The largest fold change was spot 1189 at 2.31 fold. Small but significant fold changes might arise in two ways: either they reflect uniform small fold changes, or there are nonuniform large fold changes in a subset of cells due to the high functional heterogeneity of cells within the brainstem. To address the question of region-specific expression of the gene products revealed by our screen, we compared our list of ground squirrel proteins to mRNAs that show regional expression in mouse brain. The Allen Mouse Brain Reference Atlas comprises data from in situ hybridization experiments localizing the expression of ~20,000 mRNAs in mouse brain (Lein et al. 2007). This online resource (www.brain-map.org) was searched for mRNAs that correspond to the proteins listed in Tables 1 and 2 to determine whether expression was ubiquitous or cell type-specific. Of the 85 distinct proteins examined, 76 of the gene product names matched exactly to an entry in the Allen atlas. Serial coronal sections were available for 33 of these 76; 25 demonstrated regional enrichment of expression and the other eight were ubiquitous (Table 3). These results suggest that for many proteins identified in this proteomics screen, small fold changes found in the homogenized brainstem sample are actually “diluted” representations of larger, localized fold changes. Table 4 illustrates how this heterogeneity would affect protein quantification in brainstem homogenates.

Accurate automated evaluation of large sets of biochemical data is still in its infancy. A new tool that enables statistically robust pathway searching is KEGG Spider (http://mips.gsf.de/proj/keggspider/); this was used to examine the uniquely identified proteins found to be elevated either in ET or in SA ground squirrels. By this method, using the feature to generate 200 random networks, two KEGG metabolic pathways in ET and two in SA were significantly elevated ($p<0.05$). Alanine/aspartate metabolism and the TCA cycle were elevated in ET, and pyruvate metabolism and glycolysis/gluconeogenesis were elevated in SA.

Other functional groups implicated in the present dataset include an upregulation in ET of the electron transport chain and oxidative phosphorylation, ATP synthesis machinery and components required for intracellular protein trafficking. Functional groups that contained both ET- and SA-elevated spots include protein anabolic and catabolic pathways, cytoskeleton and cell motility, redox balance and signal transduction. Changes in protein levels in all of these functional groups reveal a winter proteome that differs considerably from summer, and one which enables dynamic shifts during the torpor and arousal cycles in fuel consumption, cell survival, vesicular trafficking and cytoarchitecture (Table 5).

Discussion

Hibernators display extraordinary physiological plasticity during the winter months. They sustain core temperature as well as cardiac, respiratory and metabolic rates at one to five percent of SA levels for more than ten days at a time, then spontaneously revert to euthermic conditions that resemble summer physiology before entering another bout of torpor (reviewed in Andrews 2007; Carey et al. 2003). While ischemia and reperfusion (I/R) leads to damage, stress response and cell death in homeotherms, the brains of hibernating ground squirrels are markedly resistant to oxidative damage in spite of measurable hypoxia (Ma et al. 2005). Cells in the brain exemplify the hibernators' plasticity and resilience as they undergo transitions in activity (Kilduff et al. 1990; Krilowicz et al. 1988) and synaptic structure (Arendt et al. 2003; Ruediger et al. 2007; von der Ohe et al. 2007) during the torpor and arousal cycles of winter. As predicted, this physiological plasticity was reflected in a seasonal alteration in protein composition as measured by the changes in protein spots observed between summer and winter brainstem, a brain region containing neurons of the autonomic nervous system whose critical functions must be maintained in order to assure survival during hibernation.

This unbiased quantitative comparison of more than 2000 protein spots from 13-lined ground squirrel brainstem demonstrates that most of the proteomic complement remains unaltered between SA and ET, consistent with the maintenance of normal cellular function required throughout the year. Compared to proteomic studies in other tissues, the brainstem data revealed smaller fold changes in a larger percentage of the proteins surveyed. Thirteen percent of spots underwent a significant seasonal shift in brainstem, whereas other tissues demonstrated seasonal changes as follows: whole intestine, three percent (Martin et al. 2008); liver, 11%; lung, less than one percent; and plasma, three percent (unpublished results). Experiments using other 2DE methods also found seasonal changes in protein levels, e.g. liver, nine percent (Epperson et al. 2004), but most studies did not quantify the changes as a portion of the total. One protein in heart (Russeth et al. 2006), one protein in bat liver (Eddy et al. 2005) and six proteins in bat muscle (Lee et al. 2008) were reported to alter with hibernation state. In contrast to these other studies, almost all proteins here changed by less than two fold, likely a consequence of the extreme regional heterogeneity in the brainstem (Tables 3 and 4). Consistent with this explanation, the relative cell type homogeneity in liver may contribute to its greater fold changes (two to five fold) for a greater percentage of the proteins found there in a comparison of SA animals to hibernators (Epperson et al. 2004).

An advantage of 2D gel analysis over traditional SDS-PAGE is the possibility for separating and identifying multiple protein isoforms derived from the same gene (Fig. 3). In most cases, various isoforms of the same protein are elevated in the same season. For example, among significantly different spots in this study, all three spots identified as synuclein were elevated in SA over ET; the same was found for peptidyl-prolyl cis-trans isomerase A (three spots), and for several others. Previous results from studies in liver and intestine reveal similar patterns (Epperson et al. 2004; Martin et al. 2008). However, in the present study, two proteins were identified that were higher in SA in one spot, and higher in ET in a separate spot. These were aconitase 2 (ACO2) and guanine nucleotide binding protein (GNAO1.) Both proteins may be subject to shifts in charge (Bota and Davies 2002; Spickett et al. 2006). This spot pattern suggests a post-translational modification in hibernation (reviewed in Storey 1997), a strategy for controlling enzyme activity likely to be used along with alterations in small molecules (Nelson et al. 2009; Serkova et al. 2007) rather than de novo gene expression for the rapid winter switches required. Examples remain sparse, although several modified proteins have been identified that might play critical roles in hibernation (reviewed in Carey et al. 2003; Chen et al. 2001; Frerichs et al. 1998; Lee et al.

2007; van Breukelen et al. 2004). Investigation of multiple winter stages and identification of specific modifications is required to reveal the importance of post-translational modification in torpor and arousal cycles.

Highly significant changes between SA and ET in brainstem proteins illuminate pathways that are likely to be critical in enabling survival during hibernation (Table 5). The well-known shift away from predominantly carbohydrate metabolism in summer (Andrews et al. 2009) is indicated by the decrease in winter of many enzymes of glycolysis/gluconeogenesis as well as an increase in alanine and aspartate metabolism. The central role of energy homeostasis in hibernation shown previously in cortex metabolite shifts (Henry et al. 2007) is further revealed by the increased abundance of numerous key proteins in both the TCA cycle and oxidative phosphorylation.

The collective winter upregulation of numerous mitochondrial proteins suggests a model for rapid ATP synthesis with selective use of a portion of the TCA cycle during hibernation, specifically the three steps that follow introduction of acetyl CoA, as depicted in Fig. 4. In this model, near the end of a euthermic interbout arousal when biochemical tasks that require higher temperatures are completed, demand for ATP tapers, allowing ATP to accumulate in the mitochondrial matrix. Elevated ATP would enable phosphorylation of key TCA cycle enzymes such as alpha-ketoglutarate dehydrogenase (OGDH), leading to inactivation by well-established mechanisms and a reduction in ATP synthesis. During torpor, TCA cycle precursors derived from ketone bodies or amino acids would accumulate in the mitochondrial matrix because the TCA enzymes are inactive. Near the end of a torpor bout after slow use and local depletion of ATP, OGDH would be dephosphorylated and thus reactivated. Isocitrate dehydrogenase (IDH3A) and pyruvate dehydrogenase (PDH) are similarly activated via dephosphorylation. A rapid shift in the activity of these three enzymes would be consistent with a predicted quick reversal of oxidative suppression at the end of torpor when T_b is still very low (reviewed in Staples and Brown 2008). The restored catalytic activity of these three enzymes would generate reducing power in the form of NADH to be taken up by the adjacent electron transport chain, a process that demonstrated a unilateral upregulation in brain in ET for several of its protein subunits. The higher winter copy number of proteins in the oxidative phosphorylation pathway would allow for rapid production of ATP during arousal from torpor when demand for energy is high and in the ensuing euthermic interbout arousal (Fig. 4).

Several additional pathways were identified as changing seasonally. Pathways of protein translation, folding and turnover were elevated in either ET or SA, indicating an elaborate and potentially protein-specific strategy for synthesis, salvage and degradation. Another of the largest functional groups represented in Table 5 is that of cytoskeleton and cell motility, consistent with dramatic cellular restructuring during hibernation. Finally, redox balance, signal transduction and clathrin-mediated vesicle formation all altered from SA to ET, with all identified proteins with roles in vesicle formation increased in winter.

The results of this study support the hypothesis that differential expression of genes common to the mammalian genome plays a major role in the biochemistry of hibernation rather than expression of novel genes not found in other, non-hibernating mammals (Srere et al. 1992). These specific protein changes provide new insights into the molecular events that orchestrate and enable survival of the remarkable physiological extremes of hibernation.

Supplementary Material

Refer to Web version on PubMed Central for supplementary material.

Acknowledgments

We thank T. Finger, K. Howell, J. Hooper and C. Nelson for helpful discussion. This work was supported by P30-DC004657 to the Rocky Mountain Taste and Smell Center, Defense Advanced Research Projects Agency W81XWH-05-2-0016 to SLM and HVC and National Institutes of Health HL089049 to SLM.

Abbreviations

T_b	core body temperature
SA	summer active
ET	early torpor

References

Andrews MT. Advances in molecular biology of hibernation in mammals. Bioessays. 2007; 29:431–40. [PubMed: 17450592]

Andrews MT, Russeth KP, Drewes LR, Henry PG. Adaptive mechanisms regulate preferred utilization of ketones in the heart and brain of a hibernating mammal during arousal from torpor. Am J Physiol Regul Integr Comp Physiol. 2009; 296:R383–93. [PubMed: 19052316]

Arendt T, Stieler J, Strijkstra AM, Hut RA, Rudiger J, Van der Zee EA, Harkany T, Holzer M, Hartig W. Reversible paired helical filament-like phosphorylation of tau is an adaptive process associated with neuronal plasticity in hibernating animals. J Neurosci. 2003; 23:6972–81. [PubMed: 12904458]

Benjamini Y, Hochberg Y. Controlling the False Discovery Rate: A Practical and Powerful Approach to Multiple Testing. Journal of the Royal Statistical Society Series B (Methodological). 1995; 57:289–300.

Bernard KR, Jonscher KR, Resing KA, Ahn NG. Methods in functional proteomics: two-dimensional polyacrylamide gel electrophoresis with immobilized pH gradients in-gel digestion and identification of proteins by mass spectrometry. Methods Mol Biol. 2004; 250:263–82. [PubMed: 14755094]

Bitting L, Sutin EL, Watson FL, Leard LE, O'Hara BF, Heller HC, Kilduff TS. C-fos mRNA increases in the ground squirrel suprachiasmatic nucleus during arousal from hibernation. Neurosci Lett. 1994 Jan 3.165:117–21. [PubMed: 8015710]

Bota DA, Davies KJ. Lon protease preferentially degrades oxidized mitochondrial aconitase by an ATP-stimulated mechanism. Nat Cell Biol. 2002; 4:674–80. [PubMed: 12198491]

Bratincsák A, McMullen D, Miyake S, Toth ZE, Hallenbeck JM, Palkovits M. Spatial and temporal activation of brain regions in hibernation: c-fos expression during the hibernation bout in thirteen-lined ground squirrel. J Comp Neurol. 2007; 505:443–58. [PubMed: 17912746]

Carey HV, Andrews MT, Martin SL. Mammalian hibernation: cellular and molecular responses to depressed metabolism and low temperature. Physiol Rev. 2003; 83:1153–81. [PubMed: 14506303]

Chen Y, Matsushita M, Nairn AC, Damuni Z, Cai D, Frerichs KU, Hallenbeck JM. Mechanisms for increased levels of phosphorylation of elongation factor-2 during hibernation in ground squirrels. Biochemistry. 2001; 40:11565–11570. [PubMed: 11560506]

Dave KR, Prado R, Raval AP, Drew KL, Perez-Pinzon MA. The arctic ground squirrel brain is resistant to injury from cardiac arrest during euthermia. Stroke. 2006; 37:1261–5. [PubMed: 16574920]

Eddy SF, McNally JD, Storey KB. Up-regulation of a thioredoxin peroxidase-like protein, proliferation-associated gene, in hibernating bats. Arch Biochem Biophys. 2005; 435:103–11. [PubMed: 15680912]

Epperson LE, Dahl TA, Martin SL. Quantitative analysis of liver protein expression during hibernation in the golden-mantled ground squirrel. Mol Cell Proteomics. 2004; 3:920–33. [PubMed: 15266006]

Epperson LE, Martin SL. Quantitative assessment of ground squirrel mRNA levels in multiple stages of hibernation. Physiol Genomics. 2002; 10:93–102. [PubMed: 12181366]

Fleck CC, Carey HV. Modulation of apoptotic pathways in intestinal mucosa during hibernation. Am J Physiol Regul Integr Comp Physiol. 2005; 289:R586–R595. [PubMed: 15831769]

Frerichs KU, Hallenbeck JM. Hibernation in ground squirrels induces state and species-specific tolerance to hypoxia and aglycemia: an in vitro study in hippocampal slices. Journal of Cerebral Blood Flow and Metabolism. 1998; 18:168–175. [PubMed: 9469159]

Frerichs KU, Smith CB, Brenner M, DeGracia DJ, Krause GS, Marrone L, Dever TE, Hallenbeck JM. Suppression of protein synthesis in brain during hibernation involves inhibition of protein initiation and elongation. Proc Natl Acad Sci, USA. 1998; 95:14511–14516. [PubMed: 9826731]

Helgen KM, Cole FR, Helgen LE, Wilson DE. Generic Revision in the Holarctic Ground Squirrel Genus *Spermophilus*. Journal of Mammalogy. 2009; 90:270–305.

Henry PG, Russeth KP, Tkac I, Drewes LR, Andrews MT, Gruetter R. Brain energy metabolism and neurotransmission at near-freezing temperatures: in vivo (1)H MRS study of a hibernating mammal. J Neurochem. 2007; 101:1505–15. [PubMed: 17437538]

Karp NA, Spencer M, Lindsay H, O'Dell K, Lilley KS. Impact of replicate types on proteomic expression analysis. J Proteome Res. 2005; 4:1867–71. [PubMed: 16212444]

Kilduff TS, Miller JD, Radeke CM, Sharp FR, Heller HC. 14C-2-deoxyglucose uptake in the ground squirrel brain during entrance to and arousal from hibernation. J Neurosci. 1990; 10:2463–75. [PubMed: 2376782]

Kilduff TS, Sharp FR, Heller HC. [14C]2-deoxyglucose uptake in ground squirrel brain during hibernation. J Neurosci. 1982; 2:143–57. [PubMed: 6278102]

Krilowicz BL, Glotzbach SF, Heller HC. Neuronal activity during sleep and complete bouts of hibernation. Am J Physiol. 1988; 255:R1008–19. [PubMed: 3202216]

Lee K, Park JY, Yoo W, Gwag T, Lee JW, Byun MW, Choi I. Overcoming muscle atrophy in a hibernating mammal despite prolonged disuse in dormancy: proteomic and molecular assessment. J Cell Biochem. 2008; 104:642–56. [PubMed: 18181155]

Lee YJ, Miyake S, Wakita H, McMullen DC, Azuma Y, Auh S, Hallenbeck JM. Protein SUMOylation is massively increased in hibernation torpor and is critical for the cytoprotection provided by ischemic preconditioning and hypothermia in SHSY5Y cells. J Cereb Blood Flow Metab. 2007; 27:950–62. [PubMed: 16955077]

Lein ES, Hawrylycz MJ, Ao N, Ayres M, Bensinger A, Bernard A, Boe AF, Boguski MS, Brockway KS, Byrnes EJ, Chen L, Chen L, Chen TM, Chin MC, Chong J, Crook BE, Czaplinska A, Dang CN, Datta S, Dee NR, Desaki AL, Desta T, Diep E, Dolbeare TA, Donelan MJ, Dong HW, Dougherty JG, Duncan BJ, Ebbert AJ, Eichele G, Estin LK, Faber C, Facer BA, Fields R, Fischer SR, Fliss TP, Frensley C, Gates SN, Glattfelder KJ, Halverson KR, Hart MR, Hohmann JG, Howell MP, Jeung DP, Johnson RA, Karr PT, Kawal R, Kidney JM, Knapik RH, Kuan CL, Lake JH, Laramee AR, Larsen KD, Lau C, Lemon TA, Liang AJ, Liu Y, Luong LT, Michaels J, Morgan JJ, Morgan RJ, Mortrud MT, Mosqueda NF, Ng LL, Ng R, Orta GJ, Overly CC, Pak TH, Parry SE, Pathak SD, Pearson OC, Puchalski RB, Riley ZL, Rockett HR, Rowland SA, Royall JJ, Ruiz MJ, Sarno NR, Schaffnit K, Shapovalova NV, Sivisay T, Slaughterbeck CR, Smith SC, Smith KA, Smith BI, Sodt AJ, Stewart NN, Stumpf KR, Sunkin SM, Sutram M, Tam A, Teemer CD, Thaller C, Thompson CL, Varnam LR, Visel A, Whitlock RM, Wohnoutka PE, Wolkey CK, Wong VY, Wood M, Yaylaoglu MB, Young RC, Youngstrom BL, Yuan XF, Zhang B, Zwingman TA, Jones AR. Genome-wide atlas of gene expression in the adult mouse brain. Nature. 2007; 445:168–76. [PubMed: 17151600]

Lyman, CP.; Willis, JS.; Malan, A.; Wang, LCH. Hibernation and Torpor in Mammals and Birds. New York: Academic Press; 1982.

Ma Y, Wu S. Simultaneous measurement of brain tissue oxygen partial pressure, temperature, and global oxygen consumption during hibernation, arousal, and euthermy in non-sedated and non-anesthetized Arctic ground squirrels. J Neurosci Methods. 2008; 174:237–44. [PubMed: 18722471]

Ma YL, Zhu X, Rivera PM, Toien O, Barnes BM, LaManna JC, Smith MA, Drew KL. Absence of cellular stress in brain after hypoxia induced by arousal from hibernation in Arctic ground squirrels. Am J Physiol Regul Integr Comp Physiol. 2005; 289:R1297–306. [PubMed: 15976308]

Marouga R, David S, Hawkins E. The development of the DIGE system: 2D fluorescence difference gel analysis technology. Anal Bioanal Chem. 2005; 382:669–78. [PubMed: 15900442]

Martin, SL.; Dahl, T.; Epperson, LE. Slow loss of protein integrity during torpor: a cause for arousal?. In: BB; CHV, editors. Life in the Cold. Vol. 12. Fairbanks, AK: 2004. p. 199-208.

Martin, SL.; Epperson, LE. A two-switch model for mammalian hibernation. In: Lovegrove, BG.; McKechnie, AE., editors. Hypometabolism in Animals. Pietermaritzburg: Interpak Books; 2008. p. 177-186.

Martin SL, Epperson LE, Rose JC, Kurtz CC, Ane C, Carey HV. Proteomic analysis of the winter-protected phenotype of hibernating ground squirrel intestine. Am J Physiol Regul Integr Comp Physiol. 2008; 295:R316–28. [PubMed: 18434441]

Milsom WK, Zimmer MB, Harris MB. Regulation of cardiac rhythm in hibernating mammals. Comp Biochem Physiol A Mol Integr Physiol. 1999; 124:383–91. [PubMed: 10682236]

Nelson CJ, Otis JP, Martin SL, Carey HV. Analysis of the hibernation cycle using LC-MS-based metabolomics in ground squirrel liver. Physiol Genomics. 2009; 37:43–51. [PubMed: 19106184]

Ruediger J, Van der Zee EA, Strijkstra AM, Aschoff A, Daan S, Hut RA. Dynamics in the ultrastructure of asymmetric axospinous synapses in the frontal cortex of hibernating European ground squirrels (Spermophilus citellus). Synapse. 2007; 61:343–52. [PubMed: 17318885]

Russeth KP, Higgins L, Andrews MT. Identification of proteins from non-model organisms using mass spectrometry: application to a hibernating mammal. J Proteome Res. 2006; 5:829–39. [PubMed: 16602690]

Serkova NJ, Rose JC, Epperson LE, Carey HV, Martin SL. Quantitative analysis of liver metabolites in three stages of the circannual hibernation cycle in 13-lined ground squirrels by NMR. Physiol Genomics. 2007; 31:15–24. [PubMed: 17536023]

Spickett CM, Pitt AR, Morrice N, Kolch W. Proteomic analysis of phosphorylation, oxidation and nitrosylation in signal transduction. Biochim Biophys Acta. 2006; 1764:1823–41. [PubMed: 17070740]

Srere HK, Wang LC, Martin SL. Central role for differential gene expression in mammalian hibernation. Proc Natl Acad Sci, USA. 1992; 89:7119–7123. [PubMed: 1379733]

Staples JF, Brown JC. Mitochondrial metabolism in hibernation and daily torpor: a review. J Comp Physiol [B]. 2008; 178:811–27.

Storey KB. Metabolic regulation in mammalian hibernation: enzyme and protein adaptations. Comp Biochem Physiol. 1997; 118A:1115–1124.

Tøien Ø, Drew KL, Chao ML, Rice ME. Ascorbate dynamics and oxygen consumption during arousal from hibernation in Arctic ground squirrels. Am J Physiol Regul Integr Comp Physiol. 2001; 281:R572–83. [PubMed: 11448862]

van Breukelen F, Sonenberg N, Martin SL. Seasonal and state dependent changes of eIF4E and 4E-BP1 during mammalian hibernation: implications for the control of translation during torpor. Am J Physiol Regul Integr Comp Physiol. 2004; 287:R349–53. [PubMed: 15059792]

von der Ohe CG, Garner CC, Darian-Smith C, Heller HC. Synaptic protein dynamics in hibernation. J Neurosci. 2007; 27:84–92. [PubMed: 17202475]

Yan J, Barnes BM, Kohl F, Marr TG. Modulation of gene expression in hibernating arctic ground squirrels. Physiol Genomics. 2008; 32:170–81. [PubMed: 17925484]

Zhao HW, Christian SL, Castillo MR, Bult-Ito A, Drew KL. Distribution of NMDA receptor subunit NR1 in arctic ground squirrel central nervous system. J Chem Neuroanat. 2006; 32:196–207. [PubMed: 17097266]

Zhou F, Zhu X, Castellani RJ, Stimmelmayr R, Perry G, Smith MA, Drew KL. Hibernation, a model of neuroprotection. Am J Pathol. 2001; 158:2145–2151. [PubMed: 11395392]

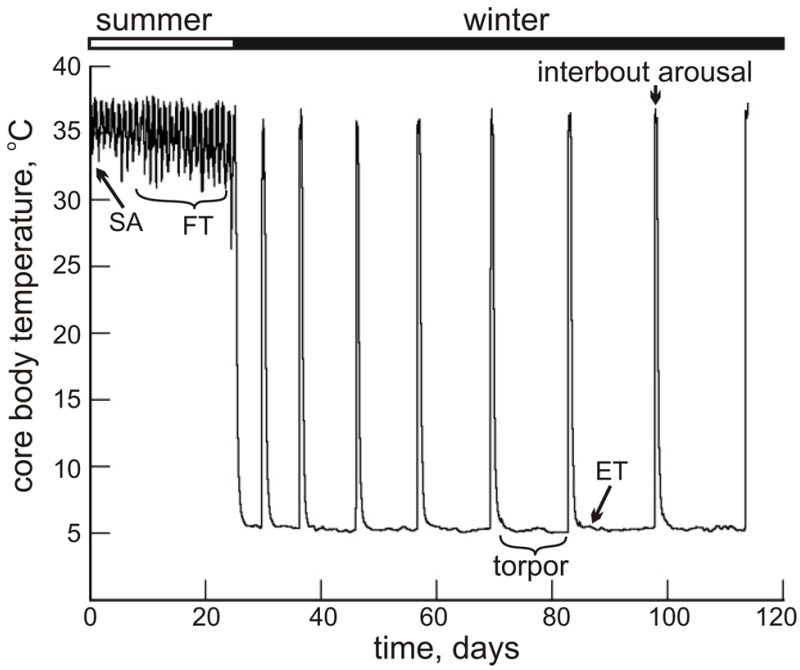

Fig. 1.

Body temperature (T_b) of a 13-lined ground squirrel for several weeks in late fall and into the first three months of winter heterothermy, i.e. hibernation; SA, summer active; FT, fall transition; ET, early torpor.

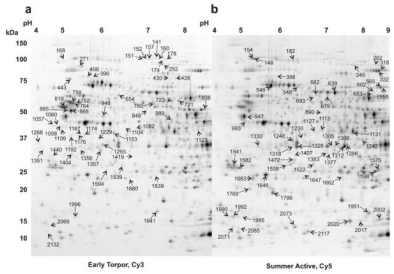

Fig. 2.

Brainstem protein differences between SA and ET. Two different Cy images from a single gel separation of soluble 13-lined ground squirrel brainstem proteins by 2DE are shown. **(a)** ET brainstem proteins labeled with Cy3, master numbers are indicated for spots elevated in ET. **(b)** SA proteins labeled with Cy5, master numbers are indicated for spots elevated in SA over ET. On the left side of the figure are markers of approximate molecular mass in kDa, and across the top are indicated the approximate isoelectric (pI) values in pH.

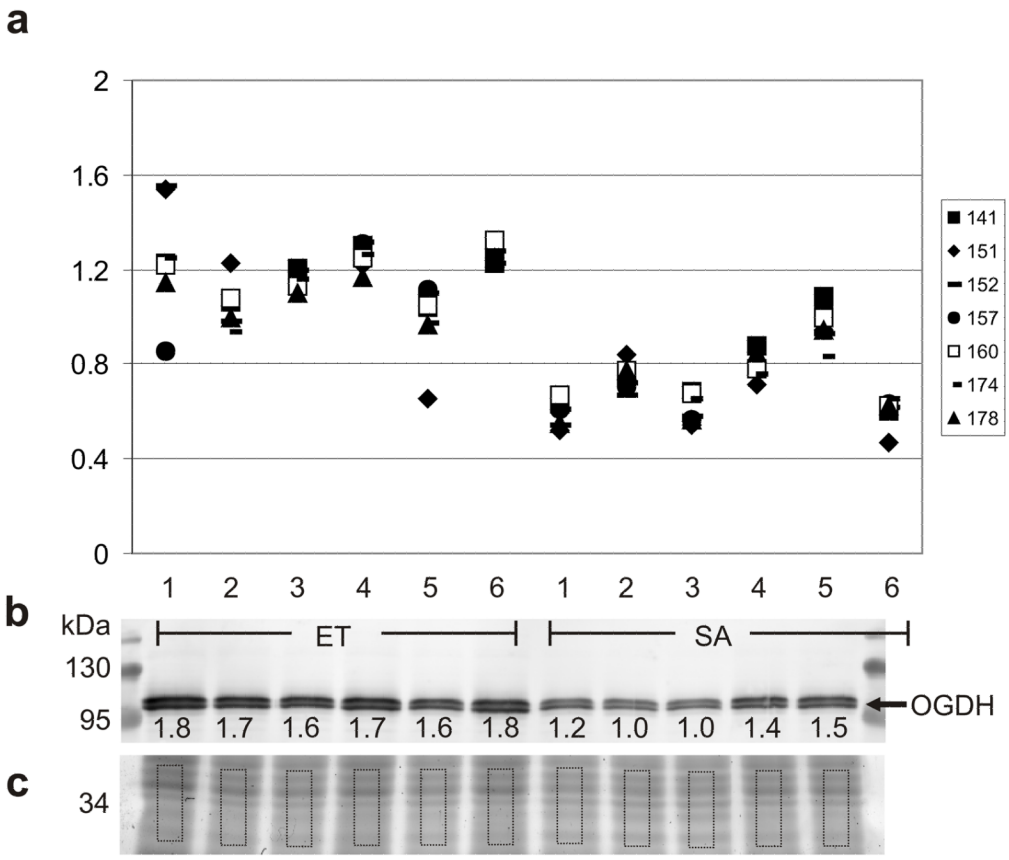

Fig. 3.

Comparison of DIGE and western quantitation for OGDH. **(a)** Isoform-specific quantitation using the normalized spot volumes obtained by DIGE of seven 2D gel spots for which OGDH was the uniquely identified protein; symbols represent protein spots as indicated; ET: n=6, SA: n=6; fold changes and Student's t-test p values for each of the seven OGDH spots are in Table 1. DIGE values are aligned with western blot lanes, except for the depleted SA6. **(b)** Western blot distinguishes two isoforms of OGDH at ~114kDa; after electrophoretic separation, the protein gel was cut and proteins in the top portion were transferred for immunoblotting, the bottom **(c)** was stained with Sypro Ruby. Molecular mass is indicated in kDa, normalized volumes are indicated under each band after correction for protein loading to the volume of the corresponding rectangle in the Sypro Ruby-stained portion of gel. Fold change for OGDH (combined bands) as determined by western, 1.39X (ET>SA); ET: n=6, SA: n=5; $p<0.0006$, Student's t-test.

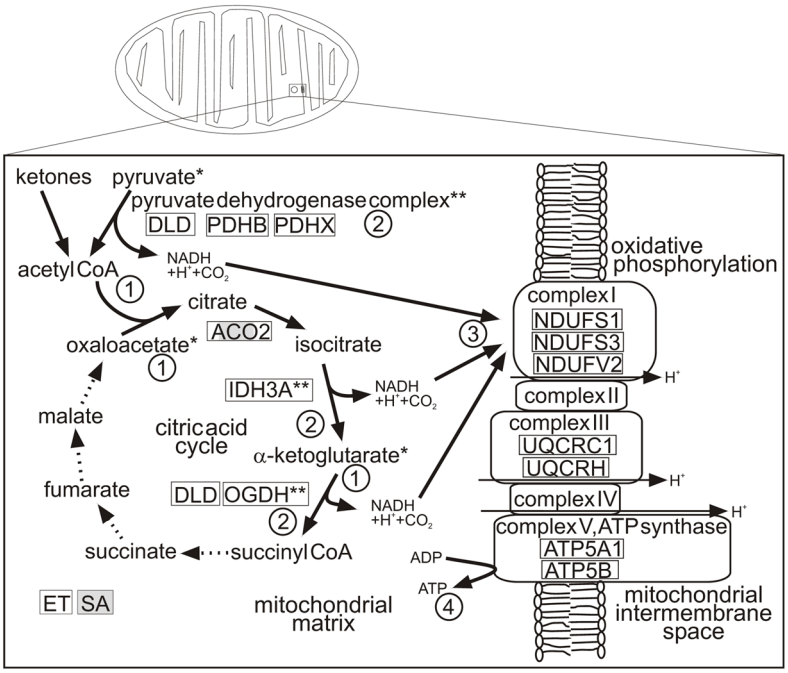

Fig. 4.

A model for rapid ATP production in hibernation, specifically during arousal from torpor and in interbout arousal. Unshaded boxes, unique ids elevated in ET; shaded boxes, unique ids reduced in ET. Aconitase 2 (partially shaded) was found in 3 spots, one was elevated in ET and two were reduced in ET. *, derived from amino acids; **, activity reversible by phosphorylation where phosphorylated form is inactive and dephosphorylation activates the enzyme. Circled numbers represent the succession of events. 1) During a torpor bout, intermediates of the citric acid (TCA) cycle accumulate and ATP stores in the mitochondrial matrix are slowly consumed until 2) ATP concentrations are depleted to a threshold resulting in dephosphorylation and therefore activation of several key metabolic enzymes. 3) Catalysis of stockpiled intermediates rapidly creates reducing power in the form of NADH which is taken up by the adjacent electron transport chain and 4) converted to ATP.

Table 1

Proteins higher in ET. ET, n=6; SA, n=6; q<0.05. Listed are the 58 spots for which a unique ID was recovered based on criteria summarized in methods. Columns are as follows: master number of spot (spot), average normalized volume ratio of ET to SA (fold), False Discovery Rate-modified p-value for the t-test (q), identification of match (protein ID), official symbol (gene), NCBI GenInfo Identifier (GI), species for this GI (species), molecular mass in Daltons for this GI (Da), number of distinct peptides matched (peps), Spectrum Mill protein score (score), amino acid coverage with ratio of quantity of recovered amino acids over total amino acids in the first column and percent coverage in the second column (AA coverage), possible area of function based on information from NCBI "gene" (functional grouping); Ub, ubiquitin; ER, endoplasmic reticulum; UPR, unfolded protein response; TCA, tricarboxylic acid cycle; ROS, reactive oxygen species; dev, development

spot	fold	q	protein ID	gene	GI	species	Da	peps	score	AA coverage		functional grouping
141	1.53	0.02	oxoglutarate dehydrogenase	OGDH	29145087	mouse	116118	4	58	55/1019	5	TCA cycle, lysine degradation, tryptophan metabolism
151	1.75	0.048	oxoglutarate dehydrogenase-like	OGDH	8922716	human	114480	5	84	76/1010	8	TCA cycle, lysine degradation, tryptophan metabolism
152	1.82	0.012	alpha-ketoglutarate dehydrogenase-like	OGDH	160419019	human	114482	13	207	166/1010	16	TCA cycle, lysine degradation, tryptophan metabolism
157	1.54	0.033	alpha-ketoglutarate dehydrogenase-like	OGDH	160419019	human	114482	7	114	100/1010	10	TCA cycle, lysine degradation, tryptophan metabolism
160	1.56	0.012	fragment: oxoglutarate dehydrogenase	OGDH	90076414	macaque	40206	2	31	22/358	6	TCA cycle, lysine degradation, tryptophan metabolism
168	1.39	0.017	ubiquitin specific peptidase 5 (isopeptidase T)	USP5	74150576	mouse	93355	9	136	109/835	13	Ub mediated protein catabolism, metal ion binding
174	1.61	0.012	ogdh protein	OGDH	29145087	mouse	116118	4	58	55/1019	5	TCA cycle, lysine degradation, tryptophan metabolism
178	1.53	0.02	oxoglutarate dehydrogenase (lipoamide)	OGDH	85861164	mouse	116450	15	220	147/1023	14	TCA cycle, lysine degradation, tryptophan metabolism
252	1.41	0.019	dynamin 1	DNM1	18093102	rat	95928	18	276	201/851	24	receptor-mediated endocytosis
271	1.33	0.045	valosin-containing protein	VCP	30023842	mouse	89364	23	354	303/806	38	caspase activation, ER UPR, protein localization
396	1.29	0.044	aconitase 2, mitochondrial	ACO2	27806769	cow	85358	28	471	314/780	40	TCA cycle, precursor metabolites
406	1.63	0.029	NADH dehydrogenase (ubiquinone) Fe-S protein 1	NDUFS1	67970033	macaque	79549	15	240	186/727	26	ETC, ATP metabolism, apoptosis, ROS metabolism
426	1.92	0.012	N-ethylmaleimide-sensitive factor	NSF	10257494	human	82653	16	251	187/744	25	protein transport, ATP binding, hydrolase activity
430	1.87	0.012	N-ethylmaleimide-sensitive factor	NSF	10257494	human	82653	15	234	170/744	23	protein transport, ATP binding, hydrolase activity
443	1.22	0.038	78 kDa glucose-regulated protein precursor (BiP)	HSPA5	115502217	ground squirrel	72329	19	320	224/654	34	ER overload and glucose response, anti-apoptosis
654	1.16	0.024	chaperonin containing TCP1, subunit 5 (epsilon)	CCT5	194676636	cow	59615	15	241	163/541	30	ATP-dependent protein folding

spot	fold	q	protein ID	gene	GI	species	Da	peps	score	AA coverage		functional grouping
721	1.38	0.012	dihydrolipoamide dehydrogenase	DLD	75040928	orangutan	54122	11	187	133/509	26	pyruvate, alpha-ketoglutarate dehydrogenase complex
723	1.29	0.018	dihydrolipoamide dehydrogenase	DLD	75040928	orangutan	54122	7	113	90/509	18	pyruvate, alpha-ketoglutarate dehydrogenase complex
752	1.77	0.027	tubulin, alpha 1B	TUBA1B	34740335	mouse	50152	10	178	142/451	31	microtubule-based movement, protein polymerization
756	1.73	0.02	tubulin, alpha 1	TUBA1B	6755901	mouse	50136	15	258	201/451	45	microtubule-based movement, protein polymerization
760	1.26	0.019	chaperonin containing TCP1, subunit 2	CCT2	149632291	platypus	60820	11	177	128/563	23	protein folding, specifically actin and tubulin
764	1.94	0.018	tubulin alpha 6	TUBA1C	14389309	human	49896	12	199	180/449	40	microtubule-based movement, polymerization
819	1.68	0.03	tubulin, beta 2	TUBB2C	4507729	human	49907	15	249	198/445	44	microtubule-based movement, polymerization
838	1.67	0.019	ATP synthase subunit alpha, mitochondrial precursor	ATP5A1	75041057	orangutan	59781	18	283	203/553	37	oxidative phosphorylation
848	1.45	0.014	dihydrolipoamide dehydrogenase-binding protein	PDHX	90075986	macaque	54055	5	72	57/501	11	pyruvate, alpha-ketoglutarate dehydrogenase complex
865	1.97	0.014	ATP synthase, H+ transporting, mitochondrial F1 complex, beta	ATP5B	32189394	human	56560	15	250	198/529	37	oxidative phosphorylation
868	1.79	0.015	ATP synthase, H+ transporting, mitochondrial F1 complex, beta	ATP5B	28940	human	57956	11	194	144/539	27	oxidative phosphorylation
948	1.59	0.023	ubiquinol-cytochrome c reductase core protein I	UQCRC1	194041191	pig	52699	14	225	174/480	36	oxidative phosphorylation, electron transport chain
989	1.46	0.012	Tu translation elongation factor, mitochondrial	TUFM	73958590	dog	63130	14	218	170/583	29	translation in mitochondria
1057	1.61	0.019	N-myc downstream-regulated gene 2 isoform a	NDRG2	73977281	dog	40718	4	55	61/371	16	neurite outgrowth
1058	1.39	0.021	N-myc downstream-regulated gene 2 isoform a	NDRG2	73977281	dog	40718	5	75	67/371	18	neurite outgrowth
1060	1.64	0.012	fragment: 40S ribosomal protein SA (p40)	RPSA	73986556	dog	29778	7	119	89/267	33	cell growth and motility
1082	1.33	0.047	purine-rich element binding protein A	PURA	149269977	mouse	33476	6	88	100/303	33	control of DNA replication and transcription
1104	1.66	0.018	purine-rich element binding protein A	PURA	73949258	dog	42792	4	53	46/404	11	control of DNA replication and transcription
1109	1.56	0.012	arsA arsenite transporter, ATP-binding	ASNA1	73986513	dog	40091	7	102	70/360	19	anion transport
1123	1.62	0.021	creatine kinase, mitochondrial 1B	CKMT1B	57108147	dog	47076	9	137	93/417	22	energy homeostasis
1153	1.44	0.045	NAD+-isocitrate dehydrogenase, alpha subunit	IDH3A	1182011	macaque	36801	9	145	100/340	29	tricarboxylic acid cycle, rate-limiting step
1167	1.38	0.033	guanine nucleotide binding protein, alpha o isoform B	GNAO1	164607137	mouse	40037	3	44	39/354	11	signal transduction, G-protein coupled
1174	1.58	0.044	guanine nucleotide binding protein, alpha o isoform B	GNAO1	164607137	mouse	40037	9	137	110/354	31	signal transduction, G-protein coupled
1176	1.6	0.028	guanine nucleotide binding protein, alpha o isoform B	GNAO1	164607137	mouse	40037	5	80	71/354	20	signal transduction, G-protein coupled

spot	fold	q	protein ID	gene	GI	species	Da	peps	score	AA coverage		functional grouping
1192	1.19	0.039	serine/threonine kinase receptor associated protein	STRAP	57106953	dog	38533	12	196	181/350	52	RNA splicing, mRNA processing, protein binding
1229	1.99	0.014	gamma-soluble NSF attachment protein	GSNAP	73962213	dog	34588	6	93	69/311	22	intracellular protein transport, Golgi and ER
1268	1.62	0.024	clathrin, light chain (Lca)	CLTA	73971342	dog	27119	2	23	17/248	7	intracellular protein transport
1293	1.54	0.014	G protein beta 1 subunit	GNB1	984553	rat	37393	9	156	106/340	31	signal transduction, G-protein coupled
1351	1.9	0.013	clathrin, light chain (Lca)	CLTA	73953331	dog	23174	3	42	29/207	14	intracellular protein transport
1356	1.61	0.013	N-ethylmaleimide-sensitive factor attachment protein, alpha	NAPA	148232359	cow	33205	9	138	124/295	42	intracellular protein transport, Golgi and ER, brain dev.
1357	1.57	0.013	pyruvate dehydrogenase E1 component beta subunit	PDHB	73985155	dog	37218	4	56	42/341	12	glycolysis, TCA cycle
1404	1.35	0.012	annexin A5	ANXA5	57100553	dog	35944	11	151	143/321	45	anti-coagulation, signal transduction
1419	1.5	0.012	voltage-dependent anion channel 2	VDAC2	90076508	macaque	31607	4	56	43/294	15	anion transport, Eukaryotic porin
1440	1.26	0.037	tropomyosin 3	TPM3	73961103	dog	28760	14	230	90/248	36	cytoskeleton, cell motility
1539	1.25	0.02	endoplasmic reticulum protein 29	ERP29	115495555	cow	28806	3	49	32/258	12	secretory protein processing, ER lumen
1594	1.78	0.029	NADH dehydrogenase (ubiquinone) Fe-S protein 3, 30kDa	NDUFS3	73983298	dog	30158	10	182	110/263	42	ETC, ATP metabolism, apoptosis, ROS metabolism
1639	1.69	0.02	heat shock protein beta-1	HSPB1	85542053	cow	22393	2	35	26/201	13	oxidative protection, cytoskeleton, chaperone
1680	1.42	0.017	NADH dehydrogenase (ubiquinone) flavoprotein 2	NDUFV2	115502498	orangutan	27355	3	52	34/249	14	ETC/ oxidative phosphorylation
1941	1.87	0.029	cofilin 1	CFL1	73983054	dog	16812	7	117	77/149	52	cytoskeleton; actin polymerization
1996	1.59	0.021	eukaryotic translation initiation factor 5A	EIF5A	4503545	human	16832	4	61	54/154	35	protein synthesis and folding (anabolism)
2069	1.26	0.038	transcription elongation factor B (SIII), polypeptide 2	TCEB2	57088081	dog	12564	2	32	21/113	19	transcription, part of ubiquitin ligase complex
2132	1.31	0.045	chain H, Cytochrome Bc1 Complex	UQCRH	4139399	cow	9175	3	43	28/78	36	ETC, mitochondrial respiration

Table 2

Proteins lower in ET. ET, n=6; SA, n=6; q<0.05. Listed are the 61 spots for which a unique ID was recovered based on criteria summarized in methods. For explanation of columns, please see legend to Table 1, except average normalized volume is ratio of SA to ET (fold); UPR, unfolded protein response; NA, nucleic acid

spot	fold	q	protein ID	gene	GI	species	MW	peps	score	AA coverage		functional grouping
148	1.42	0.02	heat shock 70kDa protein 4 isoform 6	HSPA4	114601656	chimp	94370	48	733	306/840	36	UPR, ATP binding, nucleotide binding
154	1.42	0.035	heat shock 70 kDa protein 4	HSPA4	75061973	orangutan	94299	15	240	152/840	18	UPR, ATP binding, nucleotide binding
182	1.3	0.026	heat shock 70 kDa protein 4	HSPA4	194208465	horse	94749	16	265	223/841	27	UPR, ATP binding, nucleotide binding
245	1.28	0.019	brain glycogen phosphorylase	PYGB	21361370	human	96697	14	206	146/843	17	glycogen catabolism
262	1.26	0.028	aconitase 1	ACO1	126030781	rabbit	98344	10	154	142/888	16	iron homeostasis
318	1.22	0.029	aconitase 2, mitochondrial	ACO2	40538860	rat	85434	21	344	230/780	29	TCA cycle, precursor metabolites
332	1.21	0.021	aconitase 2, mitochondrial	ACO2	40538860	rat	85434	24	388	265/780	34	TCA cycle, precursor metabolites
398	1.26	0.025	N-acylaminoacyl-peptide hydrolase	APEH	149728649	horse	81243	7	102	79/732	11	proteolysis, serine-type endopeptidase
546	1.13	0.046	heat shock 70 kDa protein 8	HSPA8	123647	hamster	70805	25	424	283/646	44	protein folding, UPR
548	1.27	0.049	collapsin response mediator protein-2A isoform 2	DPYSL2	149746221	horse	73531	15	241	223/677	33	axon guidance,
555	1.26	0.02	transketolase	TKT	67971086	macaque	67848	8	138	109/623	18	anabolic precursors, regulation of growth
565	1.27	0.021	transketolase	TKT	75054695	orangutan	67897	15	236	216/623	35	anabolic precursors, regulation of growth
602	1.25	0.029	aldehyde dehydrogenase 4 family, member A1	ALDH4A1	194207963	horse	62073	10	159	128/562	23	arginine, proline, glutamate metabolism
639	1.27	0.035	collapsin response mediator protein-2A isoform 2	DPYSL2	149746221	horse	73531	20	348	274/677	40	axon guidance
653	1.37	0.012	dihydropyrimidinase-like 5	DPYSL5	62822083	human	52094	9	140	112/477	23	nervous system dev., cone guidance
662	1.37	0.017	dihydropyrimidinase-like 3	DPYSL3	4503379	human	61964	10	139	143/570	25	nervous system dev., NA metabolism
679	1.24	0.012	dihydropyrimidinase related protein-3	DPYSL3	73949646	dog	94582	7	97	84/881	10	nervous system dev., NA metabolism
693	1.34	0.016	dihydropyrimidinase related protein-2	DPYSL2	73993705	dog	62262	13	200	180/572	31	axon guidance,
890	1.47	0.048	galactokinase 2	GALK2	11041513	macaque	40195	2	29	25/363	7	galactose metabolism
947	1.26	0.038	enolase 2	ENO2	5803011	human	47269	11	178	175/434	40	glycolysis
993	1.27	0.014	branched chain aminotransferase 1, cytosolic	BCAT1	73997380	dog	48242	3	41	21/437	5	protein anabolism/ nitrogen metabolism
1112	1.29	0.029	serpin peptidase inhibitor, clade B (ovalbumin), member 1	SERPINB1	13489087	human	42742	2	33	21/379	6	serine protease inhibitor
1127	1.35	0.035	guanine nucleotide binding protein	GNAO1	164607137	mouse	40037	6	84	74/354	21	signal transduction
1131	1.23	0.035	aldolase C, fructose-bisphosphate	ALDOC	74355075	human	43010	16	262	174/398	44	glycolysis
1230	1.48	0.012	aldolase C	ALDOC	229506	rabbit	39019	2	30	36/361	10	glycolysis
1242	1.26	0.014	aldo-keto reductase family 1, member A1 isoform 2	AKR1A1	109020298	macaque	36631	6	101	64/325	20	aldehyde catabolism

spot	fold	q	protein ID	gene	GI	species	MW	peps	score	AA coverage		functional grouping
1248	1.22	0.018	dimethylarginine dimethylaminohydrolase 1	DDAH1	57088769	dog	31307	7	112	72/285	25	nitric oxide generation
1286	1.38	0.026	aldo-keto reductase family 1, member B3	AKR1B3	160707894	mouse	35732	7	103	57/316	18	aldose reductase
1305	1.41	0.027	malate dehydrogenase 1, NAD (soluble)	MDH1	31982178	mouse	36468	3	46	31/334	9	upstream of TCA cycle, cytosolic
1306	1.35	0.043	malate dehydrogenase 1, NAD (soluble)	MDH1	31982178	mouse	36468	5	77	67/334	20	upstream of TCA cycle, cytosolic
1312	1.38	0.024	malate dehydrogenase 1, NAD (soluble)	MDH1	92087001	mouse	36511	7	98	75/334	22	upstream of TCA cycle, cytosolic
1318	1.37	0.012	lactate dehydrogenase B	LDHB	4557032	human	36639	7	109	86/334	26	glycolysis, pyruvate to lactate
1328	1.45	0.015	lactate dehydrogenase B	LDHB	4557032	human	36639	16	268	157/334	47	glycolysis, pyruvate to lactate
1330	1.42	0.019	pyridoxal (pyridoxine, vitamin B6) phosphatase	PDXP	109127253	macaque	47912	6	91	69/453	15	glycolysis, catabolism of vitamin B6
1377	1.37	0.013	pirin	PIR	57111643	dog	32150	4	57	43/290	15	transcription
1383	1.21	0.019	proteasome 26S subunit, non-ATPase, 14	PSMD14	74004396	dog	33384	2	29	23/299	8	protein turnover
1407	1.17	0.037	pyridoxal (pyridoxine, vitamin B6) phosphatase	PDXP	10092677	human	31698	6	89	62/296	21	glycolysis, catabolism of vitamin B6
1472	1.27	0.012	3-hydroxyisobutyrate dehydrogenase	HIBADH	114612561	chimp	30295	7	120	71/287	25	valine catabolism, mitochondrial
1522	1.31	0.037	haloacid dehalogenase-like hydrolase domain containing 2	HDHD2	57089151	dog	28942	3	50	40/263	15	redox
1538	1.24	0.022	chloride intracellular channel 4	CLIC4	7330335	human	28772	6	85	70/253	28	membrane potential
1541	1.14	0.018	14-3-3 protein gamma	YWHAG	71153781	cow	28253	9	144	102/247	41	signal transduction
1575	2.2	0.044	glutathione S-transferase mu 2	GSTM2	13936373	guinea pig	25695	5	75	40/218	18	glutathione-mediated detoxification
1582	1.63	0.012	calbindin 2	CALB2	34098931	mouse	31373	9	139	93/271	34	calcium ion modulation
1596	1.31	0.018	triosephosphate isomerase 1 variant	TPI1	62896835	human	26713	11	204	158/249	63	glycolysis, pentose phosphate
1646	1.35	0.017	ubiquitin carboxyl-terminal esterase L1	UCHL1	114051423	cow	28336	11	182	145/252	58	stress response, walking and eating behaviors
1647	1.33	0.029	hypoxanthine phosphoribosyltransferase 1	HPRT1	4504483	human	24580	2	27	26/218	12	purine metabolism
1662	1.35	0.018	protein-L-isoaspartate (D-aspartate) O-methyltransferase	PCMT1	67970625	macaque	30318	3	42	31/285	11	anabolism, substrate-specific methylation
1683	1.26	0.037	Rho GDP dissociation inhibitor (GDI) alpha	ARHGDIA	31982030	mouse	23408	5	80	55/204	27	signal transduction
1768	1.17	0.037	glyoxalase I	GLO1	134085635	cow	20766	2	21	14/184	8	apoptosis/anti-apoptosis
1796	1.24	0.024	peroxiredoxin 2 isoform 1	PRDX2	109123569	macaque	19470	8	138	80/176	45	redox
1951	1.29	0.012	cofilin 2	CFL2	14719392	human	18737	6	98	68/166	41	cytoskeleton; actin polymerization
1990	1.37	0.033	synuclein, gamma	SNCG	90110074	human	13331	3	46	37/127	29	cell motility, metastasis
1992	1.51	0.024	synuclein, gamma	SNCG	149034108	rat	13046	6	97	53/123	43	cell motility, metastasis
1995	1.41	0.018	synuclein, gamma	SNCG	90110074	human	13331	2	30	37/127	29	cell motility, metastasis
2002	1.23	0.024	peptidylprolyl isomerase A	PPIA	6679439	mouse	17971	5	75	47/164	29	chaperone-dependent protein folding
2017	1.28	0.025	peptidylprolyl isomerase A	PPIA	74146841	mouse	17944	4	59	31/164	19	chaperone-dependent protein folding

spot	fold	q	protein ID	gene	GI	species	MW	peps	score	AA coverage		functional grouping
2020	1.19	0.045	peptidylprolyl isomerase A	PPIA	73962252	dog	17969	2	26	18/164	11	chaperone-dependent protein folding
2071	1.56	0.012	phosphoprotein enriched in astrocytes 15	PEA15	74006311	dog	15781	3	51	27/137	20	apoptosis/anti-apoptosis
2073	1.27	0.05	programmed cell death 5	PDCD5	73948546	dog	15465	2	27	25/138	18	apoptosis/anti-apoptosis
2085	1.6	0.024	phosphoprotein enriched in astrocytes 15	PEA15	74006311	dog	15781	3	46	36/137	26	apoptosis/anti-apoptosis
2117	1.25	0.013	profilin 2	PFN2	16753215	human	15046	4	59	37/140	26	cytoskeleton; actin polymerization

J Comp Physiol B. Author manuscript; available in PMC 2011 June 16.

Table 3

Distribution in mouse brain of gene products that differ between SA and ET brains. Listed are official symbol (gene) from Tables 1 and 2 that exactly matched those of the mRNA in situ hybridization data in the Allen brain expression atlas for brainstem regions midbrain, pons and medulla for which a coronal section series was available. Specific areas of mRNA hybridization are listed (brainstem nuclei.)
Abbreviations: 3N: oculomotor nucleus, 6N: abducens nucleus, 5N: motor trigeminal nucleus, 12N: hypoglossal nucleus, 10N: dorsal motor nucleus of the vagus, AmbSC: subcompact nucleus ambiguus, AP: area postrema, ATg: anterior tegmental nucleus, CLi: caudal linear nucleus of the raphe, DR: dorsal raphe nucleus, Gi: gigantocellular reticular nucleus, LC: locus coeruleus, LDTg: laterodorsal tegmental nucleus, LPB: lateral parabrachial nucleus, LPNE: lateral parabrachial nucleus, external; LRt: lateral reticular nucleus, LSO: lateral superior olivary nucleus, IOB: inferior olive, subnucleus C of medial nucleus, IOC: inferior olive, subnucleus C of medial nucleus, IOM: inferior olive medial nucleus, me5: mesencephalic trigeminal tract, P5: peritrigeminal zone, Pn: pontine nuclei, PO: periolivary nuclei, RLi: raphe rostral linear nucleus, RMC: red nucleus, magnocellular part, ROb: raphe obscuris nucleus, RR: retrorubral nucleus, RtTg: reticulotegmental nucleus pons, scp: superior cerebellar peduncle, SNL: Substantia nigra, lateral part, Sp5C: spinal trigeminal nucleus caudal, SubB: Subbrachial nucleus.

gene	brainstem nuclei
ACO1	AmbSC
AKR1B3	LC, 10N
ALDOC	AmbSC
ANXA5	AmbSC, 10N, 12N
ARHGDIA	AmbSC, 10N, 12N
ATP5A1	ubiquitous
BCAT1	AP, 12N
CALB2	Pn, LPNE, IOC, IOB
CCT2	ubiquitous
CKMT1B	ubiquitous
CLIC4	ubiquitous
CLTA	5N, 12N
DPYSL3	LPNE, me5, 10N, 12N
DPYSL5	10N
EIF5A	me5
ERP29	me5, AmbSC, 10N
GLO1	12N, LRt
GNAO1	LDTg, light on 10N, 12N
HSPB1	P5, LSO, AmbSC, 12N
NDRG2	ROb

gene	brainstem nuclei
NDUFS1	ubiquitous
NDUFV2	Pn, Gi
NSF	ubiquitous
PEA15	CLi, LPB, LC, AmbSC, 10N, 12N
PFN2	ATg, RR, PO, 10N, 12N
PIR	12N
PYGB	6N, AmbSC, 10N, 12N
SERPINB1	RtTg, scp, Sp5C
SNCG	RLi, SNL, RMC, 3N, SubB, DR, AmbSC, 12N, 10N, IOM
UCHL1	neurons
UQCRH	ubiquitous
VDAC2	ubiquitous
YWHAG	LC, AmbSC, 10N, 12N

Table 4

Illustration of fold change dilution in homogenate for a hypothetical protein expressed in glia and in neurons of brainstem nuclei a–i. Here, glial cells are 30 times more abundant than neurons, and the protein is present at a ten fold higher copy number in neurons than in glia. The neurons in nucleus “e” increase expression of this hypothetical protein 20 fold in ET, but this fold change is reduced to 1.33 in the homogenized sample.

cell type	proportion of cells	SA	ET	scaled SA	scaled ET	fold change
glia	30	0.01	0.01	0.3	0.3	1
nuc. a	0.08	0.1	0.1	0.008	0.008	1
nuc. b	0.1	0.1	0.1	0.01	0.01	1
nuc. c	0.08	0.1	0.1	0.008	0.008	1
nuc. d	0.11	0.1	0.1	0.011	0.011	1
nuc. e	0.07	0.1	2	0.007	0.14	20
nuc. f	0.15	0.1	0.1	0.015	0.015	1
nuc. g	0.13	0.1	0.1	0.013	0.013	1
nuc. h	0.08	0.1	0.1	0.008	0.008	1
nuc. i	0.2	0.1	0.1	0.02	0.02	1
	in homogenate:			0.4	0.53	**1.33**

Table 5

Functional groupings for proteins found to alter from SA to ET. The official symbols of the genes encoding proteins that differed between SA and hibernating (ET) ground squirrels are listed.

higher in early torpor	higher in summer active
glycolysis, sugar metabolism	
	PYGB
	MDH1-cytosolic (3 spots)
	ALDOC (2 spots)
	TPI1
	ENO2
	LDHB (2 spots)
	GALK2
pyruvate dehydrogenase complex	
DLD (2 spots)	
PDHB	
PDHX	
TCA cycle	
ACO2	ACO2 (2 spots)
IDH3A	
DLD (2 spots)	
OGDH (7 spots)	
intracellular trafficking	
DNM1	
NSF (2 spots)	
GSNAP	
CLTA (clathrin, 2 spots)	
NAPA (alpha SNAP)	
signal transduction	
GNAO1 (3 spots)	GNAO1
GNB1	YWHAG (14-3-3 gamma)
ANXA5	ARHGDIA
redox	
	ACO1
	AKR1A1
	DDAH1
	AKR1B3
	HDHD2
	GSTM2
	TKT (2 spots)
	PRDX2
ion modulation	
ASNA1	CLIC4

higher in early torpor	higher in summer active
VDAC2	CALB2
cytoskeleton/cell motility	
TUBA1B (2 spots)	DPYSL2 (3 spots)
TUBA1C	DPYSL3 (2 spots)
TUBB2C	DPYSL5
NDRG2 (2 spots)	CFL2
RPSA	SNCG (3 spots)
TPM3	PFN2
HSPB1	PDXP (2 spots)
CFL1	
ETC/oxidative phosphorylation	
NDUFS1	
ATP5A1	
ATP5B (2 spots)	
UQCRC1	
NDUFS3	
NDUFV2	
UQCRH	
apoptosis/antiapoptosis	
HSPA5	GLO1
	PEA15
	PDCD5
protein synthesis and folding (anabolism)	
CCT5	HSPA4 (3 spots)
CCT2	HSPA8
TUFM	SERPINB1
ERP29	PCMT1
EIF5A	PPIA (3 spots)
protein and amino acid breakdown (catabolism)	
USP5	APEH
VCP	ALDH4A1
	PSMD14
	BCAT1
	HIBADH
	UCHL1
transcription/nucleic acid processing	
PURA (2 spots)	PIR
STRAP	HPRT1
TCEB2	